Naval Research Laboratory
Washington, DC 20375-5320

Kinetic Effects in the Chemistry of Diamond CVD Source Gases and Implications for Diamond Growth

ROBERT S. SINKOVITS

Center for Reactive Flow and Dynamical Systems
Laboratory for Computational Physics & Fluid Dynamics

C. RICHARD DEVORE

Center for Computational Physics Developments
Laboratory for Computational Physics & Fluid Dynamics

VASGEN A. SHAMAMIAN

Surface Chemistry Branch
Chemistry Division

March 22, 1996

19960411 104

REPORT DOCUMENTATION PAGE

Public reporting burden for this collection of information is estimated to average 1 hour per response, including the time for reviewing instructions, searching existing data sources, gathering and maintaining the data needed, and completing and reviewing the collection of information. Send comments regarding this burden estimate or any other aspect of this collection of information, including suggestions for reducing this burden, to Washington Headquarters Services, Directorate for Information Operations and Reports, 1215 Jefferson Davis Highway, Suite 1204, Arlington, VA 22202-4302, and to the Office of Management and Budget. Paperwork Reduction Project (0704-0188), Washington, DC 20503.

1. AGENCY USE ONLY *(Leave Blank)*	2. REPORT DATE March 22, 1996	3. REPORT TYPE AND DATES COVERED

4. TITLE AND SUBTITLE	5. FUNDING NUMBERS
Kinetic Effects in the Chemistry of Diamond CVD Source Gases and Implications for Diamond Growth	64-3780-A5 62712E

6. AUTHOR(S)

Robert S. Sinkovits, C. Richard DeVore and Vasgen A. Shamamian

7. PERFORMING ORGANIZATION NAME(S) AND ADDRESS(ES) Naval Research Laboratory Washington, DC 20375-5320	8. PERFORMING ORGANIZATION REPORT NUMBER NRL/MR/6410--96-7836

9. SPONSORING/MONITORING AGENCY NAME(S) AND ADDRESS(ES) Advanced Research Projects Agency 3701 North Fairfax Drive Arlington, VA 22203-1714	10. SPONSORING/MONITORING AGENCY REPORT NUMBER

11. SUPPLEMENTARY NOTES

12a. DISTRIBUTION/AVAILABILITY STATEMENT Approved for public release; distribution unlimited.	12b. DISTRIBUTION CODE

13. ABSTRACT *(Maximum 200 words)*

Perfectly stirred reactor calculations have been carried out on six different gas mixtures containing ethanol, water, methane, acetylene, oxygen, and hydrogen at conditions typical of low-pressure ($\sim$ 1 Torr) diamond chemical vapor deposition (CVD) reactors. For reactors operating under conditions in which the flow or diffusive time scales are short compared to the chemical time scales, the selection of viable source-gas mixtures for diamond growth based solely on the overall C-H-0 stoichiometry becomes impossible and kinetic effects must be taken into account. Numerical results are presented which show the dependence of the maximum theoretical diamond deposition rate and diamond quality as a function of mass flow rate.

14. SUBJECT TERMS Diamond growth Chemical kinetics Chemical vapor deposition			15. NUMBER OF PAGES 41
			16. PRICE CODE

17. SECURITY CLASSIFICATION OF REPORT UNCLASSIFIED	18. SECURITY CLASSIFICATION OF THIS PAGE UNCLASSIFIED	19. SECURITY CLASSIFICATION OF ABSTRACT UNCLASSIFIED	20. LIMITATION OF ABSTRACT UL

CONTENTS

KINETIC EFFECTS IN THE CHEMISTRY OF DIAMOND CVD SOURCE GASES AND IMPLICATIONS FOR DIAMOND GROWTH

I. INTRODUCTION

The growth of diamond using chemical vapor deposition has been demonstrated for a wide variety of source gases. Although methane-hydrogen remains the most common growth mixture, in recent years attention has focused on other systems containing carbon, hydrogen, and oxygen. Bachmann *et al.* [1] analyzed a large number of CVD experiments and argued that it is not the specific source gases, but rather the overall relative concentrations of the atomic species, that is critical in determining whether diamond growth is possible. The mixtures which resulted in diamond growth generally possessed C-H-O stoichiometries which fell within a well-demarcated region of the C-H-O ternary diagram as shown in Fig. 1. Defining the following variable

$$X_{C:\Sigma} = [C]/([C] + [O]), \tag{1}$$

they had determined the lower boundary separating the diamond growth and no growth regimes to be given by the line $X_{C:\Sigma} = 0.48$. The upper boundary separating the diamond growth and non-diamond carbon growth regimes is described by an arc extending from nearly the CO point to slightly above the hydrogen corner of the diagram. Bachmann *et al.* [1] were able to grow diamond from CO only if a minimum of 0.5% hydrogen was added to the gas mixture, while Saito *et al.* [2] could produce only amorphous carbon from pure CO. The shape of the diamond growth region has also been closely approximated by Prijaya *et al.* [3] using constrained thermal equilibrium calculations.

These results can be understood by assuming that the source gases have reacted for a sufficiently long time that they have lost essentially all knowledge of their initial

1

state and that a quasi-thermodynamic equilibrium has been established. The original, more complex molecules have been reduced primarily to a mixture of atomic and molecular hydrogen, small hydrocarbon species such as CH_n and C_2H_m, carbon monoxide, carbon dioxide, oxygen atoms, and hydroxyl radicals. For gas mixtures containing equal amounts of carbon and oxygen in thermodynamic equilibrium, the majority of the carbon flowed into the reactor is tied up in the form of relatively non-reactive carbon monoxide. The stability of carbon monoxide is so high that only about 1% is dissociated under conditions of 0.001 atm and 4000 K, for example. As the mixture is made more oxygen rich, atomic oxygen and hydroxyl radicals become prevalent and the system is eventually pushed into a regime in which not only is diamond growth absent, but existing diamond [4] and non-diamond carbon [5] are etched. The transition from diamond growth to non-diamond growth on the carbon-rich side of the growth region is consistent with Goodwin's analysis of a large number of CVD experiments [6]. He observed that the ratio of hydrogen atom flux to rate of carbon addition must exceed a critical value of approximately 1×10^4-3×10^4 to achieve diamond growth. Hydrogen atoms appear to be important both in creating, through hydrogen abstraction, surface radical sites where growth species can be added [7, 8], and in "annealing" the surface by promoting sp^3 bonding among carbon atoms newly added to the diamond lattice [8, 9]. With the exception of the very earliest work in diamond CVD [10, 11], all successful growth recipes have included large amounts of hydrogen.

While the assumption of quasi-thermodynamic equilibrium may be valid in typical reactors operating at relatively low flow rates and pressures of about 30 Torr and higher, it may no longer be true under operating conditions where the residence time of the source gases in the reactor is smaller than or comparable to the time required to approach thermodynamic equilibrium. In particular, our interest in these regimes

2

is motivated by the work of Rudder *et al.* [12] who demonstrated diamond growth using an ethanol-water rf-plasma discharge at a pressure of 1 Torr. Assuming that the gas-phase chemistry is dominated entirely by two-body reactions, the residence time required for the source-gas mixture to approach equilibrium scales inversely with pressure. In addition, in order to attain higher growth rates in the low pressure processes, it would be advantageous to increase the mass flow rate into the reactor thereby increasing the total amount of carbon that can be delivered to the surface. The combined effects of low pressure and high flow rate can lead to the situation described above, where the transport time scales are short compared to the chemical time scales.

Although the results described in this paper are for an operating pressure of 0.001 atm, the general trends observed also exist at higher pressures. We had shown that the characteristic chemical timescale for the formation of atomic hydrogen, carbon monoxide, and growth species from an ethanol-water mixture is inversely proportional to pressure for $P \leq 0.1$ atm [13]. In addition, the residence time within the reactor is proportional to the pressure divided by the mass flow rate $\dot{m}$. As a consequence, the species profiles at higher pressures (P^h) can be related to those at lower pressures through an appropriate change of scale in the mass flow rate, $\dot{m} \rightarrow \dot{m}(P/P^h)^2$. Since the kinetic effects are most critical for the low-pressure processes, the focus of this paper will be limited to results obtained for $P = 0.001$ atm.

The remainder of this paper is organized as follows. In the following section, we give a brief description of the elementary reaction mechanism and the approach used to carry out the perfectly stirred reactor calculations. The results of the calculations are presented for six source-gas recipes, comprising two different C-H-O stoichiometries, in section III. An analysis and explanation of the results is presented in section IV. Finally, in section V we summarize our findings.

3

II. MODEL FORMULATION

The elementary reaction set used for the calculations described in this paper is based on a combination of the acetylene combustion mechanism developed by Miller and Melius [14] and the ethanol combustion mechanism of Curran et $al.$ [15]. The acetylene mechanism has been used in a number of earlier diamond CVD simulations ($e.g.$ Meeks et $al.$ [16]). A brief description of the mechanism and its construction is presented below, but the reader is referred elsewhere [13] for a more detailed treatment.

The mechanism contains a total of 249 reversible reactions involving 54 species. All forward reaction rates are expressed in the Arrhenius form

$$k = AT^{B}e^{-E/RT}, \qquad (2)$$

and include enhanced third-body and pressure fall-off forms. The acetylene mechanism was chosen as the starting point for our reaction set since it has been extensively validated for combustion at high temperatures, T $\geq$ 3000 K, and includes a detailed treatment of the chemistry of species such as C, CH, and C_2 which are important under the range of conditions of interest in this study. A subset of the reactions from the ethanol combustion mechanism was appended to the acetylene set to handle the chemistry of ethanol and important intermediate species not explicitly treated in the acetylene mechanism. This subset includes 23 reactions directly involving ethanol and five additional reactions describing the decomposition of the species pC_2H_4OH, sC_2H_4OH, CH_3CHO, and C_2H_5O. The ethanol reaction set was originally developed to model combustion at significantly lower temperatures, T $\leq$ 2000 K, but for the purpose of this study we have assumed that the reaction rates in this mechanism can be extended to higher temperatures.

All of the calculations were performed using the Sandia CHEMKIN program

4

Perfectly Stirred Reactor (PSR) [17, 18]. The basic assumption of PSR is that the mixing of reactants is so complete that the conversion of reactants to products is totally determined by the chemical reaction rates rather than diffusion, convection or other transport processes. Fresh source gases are continuously injected into the reactor where they mix and react with the older material. This is in contrast to plug-flow reactor simulations where there is no mixing of new and old material and the time-evolution of an isolated volume of the reactants is calculated. The equations used in PSR are species conservation

$$\dot{m}(Y_k - Y_k^*) - \dot{\omega}_k W_k V = 0, \tag{3}$$

and energy conservation

$$\dot{m} \sum_{k=1}^{K} (Y_k h_k - Y_k^* h_k^*) + Q = 0, \tag{4}$$

where $\dot{m}$ is the mass flow rate through the reactor, V is the reactor volume, and Q is the reactor heat loss. The subscripted variables Y_k, W_k, h_k, and $\dot{\omega}_k$ are the mass fraction, molecular weight, specific enthalpy, and production rate, respectively, of species k. The starred variables represent inlet conditions and the summation in the energy equation is over the number of species K. The mass flow rate is related to the residence time τ in the reactor by the equation

$$\tau = \frac{\rho V}{\dot{m}}, \tag{5}$$

where ρ is the mass density in the reactor. The steady-state conservation equations are solved using a hybrid Newton/time-integration method. The PSR program can be used in one of two modes. Either the temperature and pressure of the reactor can be specified, in which case the K species conservation equations are solved, or the reactor heat loss and pressure are specified and the $K + 1$ species and energy equations are solved. In all of our simulations we assume that the reactor temperature and pressure

5

are known and use PSR to calculate the species mole fractions in the reactor for mass flow rates corresponding to residence times ranging from 1×10^{-4} s to 1×10^3 s. Since by default PSR uses the results of a thermodynamic equilibrium calculation as a first guess for the outlet gas composition, it is easy to verify that the PSR calculations agree with thermodynamics in the limit of long residence times. For nearly all of our calculations the thermodynamic equilibrium conditions are closely approached for a residence time of 1×10^3 s.

In addition to the mole fractions of individual species, we are also interested in the flow rate-dependent behavior of several derived quantities related to the distribution of carbon and hydrogen, the rate of diamond deposition, and the quality of the deposited material. For the purpose of diamond growth, we are concerned not just with the total concentration or mole fraction of the elemental species, but with the fractions of the elemental species that are available to actively participate in the diamond growth. Although there is disagreement over which hydrocarbon species are the dominant growth precursors, most studies suggest that it is the C_1 radical species, particularly methyl (CH_3). Diamond growth mechanisms based on acetylene as the active hydrocarbon species have been proposed [19–24], but numerical simulations by Coltrin and Dandy [25] suggest that the rate of diamond deposition due to acetylene is generally negligible compared to that for carbon atoms or methyl radicals. Experiments and modeling by Harris and Martin [26] suggest that the growth rate and diamond quality are significantly lower when C_2H_2 is the active growth species as compared to methyl radicals. Similar conclusions were reached by Martin and Hill [27, 28]. Because of the uncertainty in the role of C_2 species in diamond growth, we have not included them as possible diamond precursors. CH_4 was not included as a growth species because an analysis of the experiments of Chauhan *et al.* [29] by Harris [30] suggests that although CH_4 can participate directly in diamond growth, the

6

surface reaction probability for CH_4 is approximately six orders of magnitude lower than that for CH_3. We have also made the assumption that all of the C_1 radicals will play the same role in diamond growth. Under typical CVD conditions where the flux of hydrogen atoms to the surface is large compared to the C_1 radical flux, C, CH, and CH_2 species which are added to the surface should rapidly have their dangling bonds terminated by hydrogen atoms.

The fraction of carbon atoms in the system that are in the form of C_1 radicals can be defined as

$$f(C_1 \text{rad}) = \frac{\sum_{m=0}^{3} X(CH_m)}{\sum_{n=1}^{6} \sum_m \sum_p n X(C_n H_m O_p)}, \tag{6}$$

where the quantities $X(C_n H_m O_p)$ are the mole fractions of the individual species. The quantity $X(CH_2)$ accounts for both the singlet and triplet state of the methylene radical. The summation over m in the numerator restricts the contribution to radical species. In the denominator, the maximum value of n is limited to six since our reaction mechanism only contains up to C_6 chemistry. The limits for the summations over m and p are assumed to be consistent with the number of carbon atoms. Similarly, the fractions of carbon in the forms of CH_4, C_2, and heavier ($\geq C_3$) species are given by

$$f(CH_4) = \frac{X(CH_4)}{\sum_{n=1}^{6} \sum_m \sum_p n X(C_n H_m O_p)}, \tag{7}$$

$$f(C_2) = \frac{\sum_m \sum_p 2 X(C_2 H_m O_p)}{\sum_{n=1}^{6} \sum_m \sum_p n X(C_n H_m O_p)}, \tag{8}$$

and

$$f(\geq C_3) = \frac{\sum_{n=3}^{6} \sum_m \sum_p n X(C_n H_m O_p)}{\sum_{n=1}^{6} \sum_m \sum_p n X(C_n H_m O_p)}. \tag{9}$$

Another important quantity is the fraction of carbon tied up in the form of carbon monoxide and related species. Once carbon reacts to create carbon monoxide, it is

7

essentially inert and it is expected to play very little role in diamond growth, at least as compared to active radical species. Under the conditions of interest using the reaction mechanism described earlier, HCO and CO_2 undergo reactions to form exclusively CO. CH_3O leads directly to the creation of CH_2O which in turn decomposes to form HCO. CH_2OH typically reacts to form CH_2O, but at very slow flow rates, the creation of methyl radicals is observed. This path is unimportant though since the mole fractions of CH_2OH at these flow rates are less than 10^{-10}. The fraction of carbon in the form of inert species then is given by

$$f(CO) = \frac{X(CO) + X(HCO) + X(CO_2) + X(CH_2O) + X(CH_2OH) + X(CH_3O)}{\sum_{n=1}^{6} \sum_m \sum_p nX(C_nH_mO_p)}.$$

(10)

Finally, we define the fraction of hydrogen in the form of active hydrogen atoms as

$$f(H) = \frac{X(H)}{\sum_{n=0}^{6} \sum_m \sum_p mX(C_nH_mO_p)}.$$

(11)

The quality of the deposited diamond can be predicted from the relative fluxes of hydrogen atoms and growth species to the surface. An analysis of the conditions which lead to the growth of high-quality diamond indicates that a minimum of $\sim 1 \times 10^4$-3×10^4 hydrogen atoms must strike the diamond surface for every carbon atom that is incorporated on the surface [6]. If we neglect boundary layer effects and assume that all CH_m radical species have the same probability of sticking to a surface radical site, we can make the following estimate of the ratio of hydrogen atom flux to rate of carbon atom incorporation,

$$\Psi = \frac{X(H)/\sqrt{m_H}}{(\sum_{n=0}^{3} X(CH_n)/\sqrt{m_{CH_n}})\gamma Z},$$

(12)

where γ is the sticking probability and Z is the fraction of surface sites that are open. We used the values of $\gamma = 0.33$ based on the surface chemistry mechanism of

8

Coltrin and Dandy [25] and $Z = 0.085$ derived from the hydrogen atom abstraction and recombination probabilities of Brenner *et al.* [31, 32].

A maximum theoretical rate of diamond deposition can be defined as

$$D_{max} = \dot{m} Y_{\rm C} f({\rm C_1 rad}), \tag{13}$$

where $Y_{\rm C}$ is the total carbon mass fraction of the inlet gases. The dimensions of D_{max} are (mass/time) and were chosen in this way rather than in the usual dimensions of (length/time) so that the results will be independent of reactor geometry and growth area. Our expression for D_{max} is based on the assumption that C_1 radicals are converted to diamond with 100% efficiency. Obviously, this is an unrealistic assumption since it neglects the growth of non-diamond carbon, the finite transport rates of the growth species and hydrogen atoms, and the non-unity probability of incident growth species sticking to the surface. Nonethless, our definition is still useful for several reasons. First, it sets an absolute upper bound on the diamond deposition rate. Second, taken together with the quality factor defined above, it can be used to help establish optimal flow rates and reactor operating conditions. Finally, although D_{max} may be substantially larger than deposition rates that can be realistically expected, it allows us to make at least rough comparisons between different source-gas recipes.

III. RESULTS

In this section we present the results of our calculations for a variety of CVD source-gas recipes. Three of the mixtures, ethanol-water-hydrogen 21:20:1, methane-oxygen 84:41, and acetylene-oxygen-hydrogen 42:41:126, all possess the same overall C-H-O stoichiometry of 42:168:41. These mixtures, which will be referred to as CO-rich systems since they all contain large amounts of carbon and oxygen in nearly identical proportions, are labeled as "mix1" on Fig. 1. This choice of stoichiometry

was motivated by our interest in the ethanol-water system [12, 13, 33] and is just slightly carbon-rich relative to pure methanol (C-H-O = 1:4:1). A second set of three mixtures, ethanol-hydrogen 1:81, methane-oxygen-hydrogen 4:1:160, and acetylene-oxygen-hydrogen 2:1:166, all have an identical C-H-O composition of 2:168:1, with the stoichiometry chosen so as to be in the range of typical methane-oxygen-hydrogen recipes. This second set of mixtures, labeled as "mix2" on Fig. 1, will be referred to as CO-lean systems since carbon monoxide is a relatively minor component of the fully reacted gases. Our choice of nomenclature is somewhat arbitrary, but it does provide a descriptive way of differentiating the two sets. All six of the mixtures have an H/(C-O) ratio equal to 168. By choosing different gas mixtures with identical C-H-O ratios, we are able to distinguish effects due to the specific source gases from those due to the overall stoichiometry. The H/(C-O) ratio was chosen to be a constant in order to confirm that the quality factors for all six cases converge to the same value in the limit of low flow rates (long residence time).

The carbon and hydrogen distributions, diamond quality factors, and maximum theoretical deposition rates are displayed in Figs. 2-7 for the six recipes described above. In all of the simulations, the reactor volume is 1000 ℓ, the temperature is 3000 K and the pressure is 0.001 atm. For other reactor volumes, the scaled flow rate for a 1000 ℓ reactor is related to the actual flow rate by

$$\dot{m}_{1000} = \frac{1000}{V}\dot{m}. \tag{14}$$

The maximum deposition rates for two reactors operating at the same $\dot{m}/V$ ratio are related by

$$D_{max} = \frac{V}{1000}D_{max\,1000}. \tag{15}$$

For all six cases, D_{max} drops with decreasing flow rate for low flow rates, with the dependence becoming linear in the limit $\dot{m} \to 0$. This reflects a convergence to

10

thermodynamic equilibrium in the reactor vessel as $\tau \to \infty$. The deposition rate is directly proportional to the flow rate, and depends only on the overall C-H-O stoichiometry. At high flow rates, the behavior of D_{max} depends sensitively on the nature of the carbon source. Feed gases containing ethanol or acetylene both result in a well defined maximum in D_{max}, while source gases relying on methane as the carbon source lead to a deposition rate that asymptotically approaches a maximum in the limit $\dot{m} \to \infty$.

The behavior of the quality factor is slightly more complicated since it depends on both $f(C_1 \text{rad})$ and $f(H)$. In the limit $\dot{m} \to 0$, the quality factors for the six cases are independent of $\dot{m}$ and all converge to the same value, as shown in Fig. 8. Ψ exhibits a maximum in the vicinity of $\dot{m} = 10^{-2}$ g/s, but the maxima for the CO-lean mixtures are considerably more pronounced than those for the CO-rich mixtures. The most striking differences in the quality factors occur at high flow rates. With the exception of the CO-lean acetylene mixture, Ψ drops rapidly as the flow rate is increased. The quality factors for the CO-lean ethanol-hydrogen and acetylene mixtures show local minima at high flow rates, while the remaining mixtures have quality factors that drop monotonically with increasing $\dot{m}$. The details of this behavior are probably unimportant since they occur in flow regimes where Ψ is well below that required for diamond growth.

The carbon and hydrogen distributions show that in the limit $\dot{m} \to 0$, the inlet gases are converted almost entirely to carbon monoxide, atomic hydrogen and C_1 radical species as predicted by thermodynamics. At the other extreme of high flow rates, the inlet gases pass through the reactor with minimal conversion to the thermodynamically stable products. In all cases, $f(CO)$ and $f(H)$ increase steadily as the flow rate is decreased and $f(\geq C_3)$ exhibits a global maximum for intermediate flow rates. The behavior of $f(C_2)$ and $f(CH_4)$ depend on the form of the carbon source. For

11

mixtures containing ethanol or acetylene, $f(C_2)$ decreases steadily as $\dot{m} \to 0$ while $f(CH_4)$ reaches a maximum for intermediate flow rates. The characteristic behaviors of $f(C_2)$ and $f(CH_4)$ as a function of $\dot{m}$ are exchanged when methane is used as a carbon source. The most unusual trend is that shown by $f(C_1\text{rad})$ as the flow rate is varied. At first, $f(C_1\text{rad})$ rises steadily as the flow rate is decreased from infinity, but it passes through a global maximum and then a local minimum before settling to the value predicted by thermodynamic equilibrium at low flow rates.

IV. ANALYSIS

Based solely on the behavior of D_{max}, the strategy for diamond growth in a low-pressure, hot-filament or microwave-plasma reactor would appear to be straight forward: for source gases containing methane, increase the flow rate until the diamond deposition rate levels off; for recipes utilizing ethanol or acetylene, increase the flow rate until the predicted maximal growth rate is obtained. Unfortunately, two factors related directly to the gas-phase chemistry severely limit the potential growth rates. First, the quality of the deposited material depends on the ratio of atomic hydrogen to C_1 radicals. In most of the cases examined, with the notable exception of the CO-lean acetylene mixture, the C_1 radicals are created more readily than hydrogen atoms at high flow rates, leading to unfavorable values of Ψ. Second, it is believed that heavier hydrocarbon species may be responsible for the growth of non-diamond carbon. While there is uncertainty over the role of C_2 species in diamond and non-diamond carbon growth, it is likely that the heavier hydrocarbon species ($\geq C_3$) do not play a role in diamond growth and may in fact lead to the deposition of non-diamond carbon. Particularly for the CO-rich mixtures, the fraction of carbon in the form of C_3 and heavier species can be significant ($\simeq 10\%$) and considerably greater than the fraction in the form of C_1 radicals.
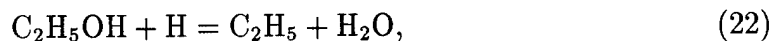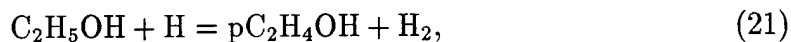
12

While the hydrogen and carbon distributions in the limit of slow flow rates are specified entirely by thermodynamics, the distributions at higher flow rates are determined by a complex interplay between a number of different mechanisms. At short residence times, the carbon fractions in the form of carbon monoxide, CH_m, and C_2H_n species can depend strongly on the dissociation pathways of the carbon-bearing source gas. As an example, we consider the chemistry of ethanol. Hydrogen atoms attack ethanol via four important reactions. Two of these,

$$C_2H_5OH + H = sC_2H_4OH + H_2, \qquad (16)$$

$$C_2H_5OH + H = C_2H_5O + H_2, \qquad (17)$$
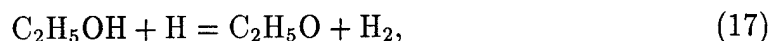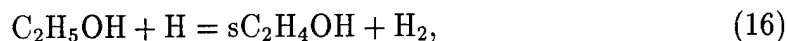
lead directly to the formation of carbon monoxide and methyl radicals via the following paths

$$sC_2H_4OH \rightarrow CH_3CHO \rightarrow HCO \rightarrow CO, \qquad (18)$$

$$sC_2H_4OH \rightarrow CH_3CHO \rightarrow CH_3CO \rightarrow CO, \qquad (19)$$

$$C_2H_5O \rightarrow CH_2O \rightarrow HCO \rightarrow CO. \qquad (20)$$
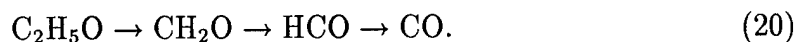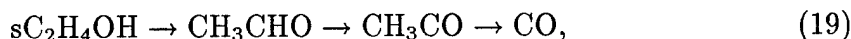
A second pair of reactions,

$$C_2H_5OH + H = pC_2H_4OH + H_2, \qquad (21)$$

$$C_2H_5OH + H = C_2H_5 + H_2O, \qquad (22)$$

result in the formation of C_2 species, either directly or through a pathway involving the unimolecular dissociation

$$pC_2H_4OH = C_2H_4 + OH. \qquad (23)$$

13

Since all four of the initial reactions in the ethanol decomposition involve the same species, the branching ratio between the formation of C_1 and C_2 species depends solely on the relative Arrhenius rates. The reaction rates and branching ratio are shown as a function of temperature in Fig. 9. As the temperature is raised above 2000 K, the formation of C_2 species becomes favored, but it should be noted that over the range 1000-4000 K, the two pathways are comparable with the branching ratio only varying from 0.7 to 1.3.

Although the dissociation pathways of the source gases can have a strong effect on the carbon and hydrogen distributions, the generic elementary reactions common to all carbon-hydrogen-oxygen mixtures are usually more important. Under the conditions of interest in this study, the dominant pathways for the creation of C_2 species from C_1 species are the reactions of the forms

$$CH_n + CH_m = C_2H_{n+m-1} + H, \tag{24}$$

$$CH_n + CH_m = C_2H_{n+m-2} + H_2. \tag{25}$$
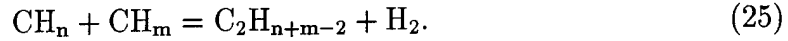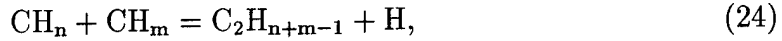
Since these are simple two-body reactions, they can proceed much more readily at low gas densities than the pressure-dependent, three-body reaction

$$CH_3 + CH_3(+M) = C_2H_6(+M), \tag{26}$$
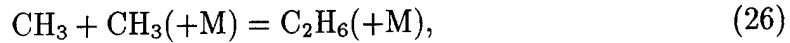
which is important for methane under typical combustion conditions. Reactions of the more general forms

$$C_nH_m + C_pH_q = C_{n+p}H_{m+q-1} + H, \tag{27}$$

$$C_nH_m + C_pH_q = C_{n+p}H_{m+q-2} + H_2, \tag{28}$$

14
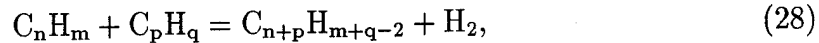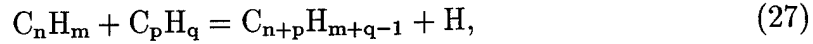
are responsible for the creation of heavier hydrocarbon species.

While only the forward directions of reactions (25) and (28) are generally important, the reverse reactions (-24) and (-27) play an important role in the pyrolysis of heavier hydrocarbons. The balance between heavy and light hydrocarbon species depends strongly on both the reaction rates and the hydrogen atom concentration. The fraction of hydrogen in the form of hydrogen atoms in turn depends on the rates of the dissociation reactions

$$H_2 + M = H + H + M, \tag{29}$$

$$RH + M = R + H + M, \tag{30}$$

and the hydrogen shuffling reactions

$$H_2 + R = RH + H, \tag{31}$$

where R is a generic hydrogen-carbon-oxygen species. The hydrogen atom-carbon radical ratio is also affected by the creation of carbon monoxide. Carbon monoxide can be formed either directly from the dissociation of the source gases, as described above for ethanol, or through the reactions involving oxygen atoms or molecules, hydroxyl radicals, and hydrocarbon species.

The carbon and hydrogen profiles in Figs. 2-7 clearly show the interplay between these various mechanisms. As an example, we consider the CO-rich methane-oxygen mixture. For this source gas recipe, methane is the only source of hydrogen. As a result, in the limit of very high flow rates, C_1 radicals and hydrogen atoms are formed at almost the same rate. Decreasing the flow rate allows the fast reactions (24,25,27,28) to occur, leading to the formation of heavier hydrocarbon species from the C_1 radicals. As the flow rate is further decreased, slower reactions which result in the formation of hydrogen atoms and carbon monoxide become more important

15

and the gas mixture asymptotically approaches the thermodynamic equilibrium composition. The minimum in $f(C_1 rad)$ at approximately $\dot{m} = 0.01$ g/s is due to the competition between the forward reactions (24,25,27,28) which consume C_1 radicals at high flow rates when $f(H)$ is low and the reverse reactions (-24,-27) which produce C_1 radicals at low flow rates when $f(H)$ is high. The behavior of D_{max} in the limit $\dot{m} \to \infty$ follows from the fact that the formation of methyl radicals at short residence times is due almost entirely to the dissociation reaction

$$CH_4 + M = CH_3 + H + M. \tag{32}$$
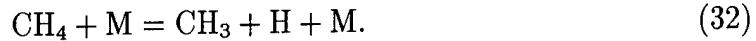
In the high-flow-rate limit, $f(C_1 rad)$ becomes directly proportional to residence time, or inversely proportional to flow rate, resulting in D_{max} independent of flow rate. Of course, since the ratio of hydrogen atoms to methyl radicals approaches unity, the growth of high-quality diamond would not be expected.

While many of the features described above for the methane-oxygen mixture are common to the other gas recipes studied, there are important qualitative differences. For the gas mixtures utilizing ethanol or acetylene as the carbon source, D_{max} exhibits a global maximum as a function of flow rate and decreases in the limit $\dot{m} \to \infty$. This is because the initial step in the dissociation of the source gases does not directly yield C_1 radicals, but rather intermediate species which must undergo further reactions before producing growth species.

The analysis up to this point has been based on the assumption that the dissociation of hydrogen is due entirely to gas-phase reactions involving neutral species. In reality, the situation is typically more complex since H_2 molecules can dissociate on the filament surfaces in hot-filament reactors or through electron-impact reactions in plasma-enhanced CVD. To account for these additional mechanisms of hydrogen dissociation, we have run a set of simulations in which the rate k_{diss} of the dissoci-

16

ation reaction (29) has been increased by factors of 10, 100, and 1000. The results for Ψ and D_{max} obtained using the ethanol-water-hydrogen and ethanol-hydrogen mixtures are displayed in Figs. 10 and 11. Both Ψ and D_{max} generally increase for a given flow rate as k_{diss} is increased, with gains of up to an order of magnitude at the largest values of k_{diss}. This has the effect of pushing the maximum flow rate at which diamond growth is expected to occur ($\Psi > 10^4$), and hence the maximum diamond growth rate, to higher values. The peak in Ψ at flow rates of approximately 0.01 g/s is seen to diminish or even vanish as k_{diss} is increased. This is due to the fact that the increased hydrogen dissociation drives the system towards thermodynamic equilibrium more quickly and reduces or eliminates the dip in $f(C_1 \text{rad})$.

V. SUMMARY

The Bachmann diagram has proven to be a very useful construct in predicting which source-gas recipes are likely candidates for diamond growth, but its utility may be limited because it does not account for important kinetic effects in the gas-phase chemistry. The fact that the diamond growth regime is determined solely by the overall C-H-O stoichiometry suggests that the source gases have been allowed to react for a relatively long time and establish a quasi-thermodynamic equilibrium before reaching the growth surface. In most diamond CVD reactors this is the case. In low-pressure, high-flow-rate reactors where the chemical reaction time scales are long or comparable to the times required for diffusion to the growth surface or flow through the reactor to occur, however, this assumption may no longer be true and kinetic effects must be taken into account.

In this paper, we have studied the effect of varying the source-gas flow rates on both the diamond quality and the theoretical maximum growth rate. We have found that increasing the gas flow rate generally increases the growth rate, but often at the

expense of material quality. At high flow rates, there can be both an unfavorable ratio of hydrogen atoms to C_1 radicals, which we have quantified in terms of Goodwin's quality parameter [6], and large concentrations of C_3 and heavier hydrocarbon species, resulting in degradation of the diamond film. For gases utilizing a C_2 carbon source, the maximum growth rate has been shown to decrease at high flow rates since the residence time in the reactor is too short to allow for the formation of potential growth species. Important quantitative differences exist between the CO-rich and CO-lean mixtures. Because the CO-rich systems contain large amounts of carbon not initially bound in the form of carbon monoxide, unfavorably high concentrations of C_3 and heavier hydrocarbon species may be built up at high flow rates.

Of the various recipes studied, the CO-lean, acetylene-oxygen-hydrogen mixture appears to be the most robust. For all flow rates, the atomic hydrogen-to-carbon radical ratio is predicted to be sufficiently large so as to yield high-quality diamond growth. Unfortunately, this result is apparently of theoretical interest only, since the explosive hazards associated with using acetylene-hydrogen mixtures in a microwave-plasma or hot-filament reactor far outway the potential benefits.

Obviously, the perfectly-stirred reactor calculations ignore many important physical processes that occur within a real diamond CVD reactor. Surface reactions will have the effect of both depleting the carbon radical population and converting atomic to molecular hydrogen. Numerical simulations taking into account plasma chemistry indicate that the electron impact dissociation of carbon monoxide may be important, resulting in a considerably larger flux of growth species to the surface [34]. The counter-diffusion of molecular hydrogen and atomic hydrogen through the boundary layer over the growth surface has also been ignored. The study of these effects is left to future work. Nonetheless, the general results derived from this study regarding the dependence of diamond quality, maximum growth rate, and gas-phase composition

on the source gases and flow rates are expected to be approximately valid.

ACKNOWLEDGMENTS

REFERENCES

[1] P.K. Bachmann, D. Leers, and H. Lydtin, Diamond Relat. Mater. **1**, 1 (1991); P.K. Bachmann, D. Leers, H. Lydtin, and D.U. Wiechert, paper 2.7, Abstr. Diamond Films '91, Nice, September 2-6, 1991; P.K. Bachmann, D. Leers, and D.U. Wiechert, paper 4.2, Abstr. Diamond, Heidelberg, August 31-September 4, 1992.

[2] Y. Saito, K. Sato, K. Gomi, and H. Miyadera, J. Mater. Sci **25**, 1246 (1990).

[3] N.A. Prijaya, J.C. Angus, and P.K. Bachmann, Diamond Relat. Mater. **3**, 129 (1993).

[4] R.E. Thomas, R.A. Rudder, and R.J. Markunas, J. Vac. Sci. Tech. A **10**, 2451 (1992).

[5] S.J. Harris and A.M. Weiner, Appl. Phys. Lett. **55**, 2179 (1989).

[6] D.G. Goodwin, private communication, 1994.

[7] B.D. Thoms, J.N. Russell, Jr., P.E. Pehrsson, and J.E. Butler, J. Chem. Phys. **100**, 8425 (1994).

[8] J.E. Butler and R.L. Woodin, Phil. Trans. R. Soc. Lond. A **342**, 209 (1993).

[9] D.G. Goodwin, J. Appl. Phys. **74**, 6888 (1993).

[10] W. Eversole, U.S. Patents 3030187, 3030188, 1962 (filed 1959).

[11] H.J. Hibsman, U.S. Patent 3371996, 1968 (filed 1964).

[12] R.A. Rudder, G.C. Hudson, J.B. Posthill, R.E. Thomas, R.C. Hendry, D.P.

Malta, R.J. Markunas, T.P. Humphreys, and R.J. Nemanich, J. Appl. Phys. **60**, 329 (1991)

[13] R.S. Sinkovits, C.R. DeVore, V.A. Shamamian, and C.K. Westbrook, Diamond Relat. Mater. **4**, 1277 (1995).

[14] J.A. Miller and C.F. Melius, Comb. Flame **91**, 21 (1992).

[15] H.J. Curran, M.P. Dunphy, J.M. Simmie, C.K. Westbrook, and W.J. Pitz, 24th Symposium (Int'l) on Combustion, Combustion Institute, 769 (1992).

[16] E. Meeks, R.J. Kee, D.S. Dandy, and M.E. Coltrin, Comb. Flame **92**, 144 (1993).

[17] P. Glarborg, R.J. Kee, J.F. Grcar, and J.A. Miller, Sandia National Laboratories Report, SAND89-8209 (1993).

[18] R.J. Kee, F.M. Rupley, and J.A. Miller, Sandia National Laboratories Report, SAND89-8009B (1994).

[19] M. Frenklach and K.E. Spear, J. Mater. Res. **3**, 133 (1988).

[20] D. Huang, M. Frenklach, and M. Maroncelli, J. Phys. Chem. **92**, 6379 (1988).

[21] M. Frenklach, J. Appl. Phys. **65**, 5142 (1989).

[22] M. Frenklach and H. Wang, Phys. Rev. **B43**, 1520 (1991).

[23] D.N. Belton and S.J. Harris, J. Chem. Phys. **96**, 2371 (1991).

[24] S.J. Harris and D.N. Belton, Jap. J. Appl. Phys. **30**, 2615 (1991).

[25] M.E. Coltrin and D.S. Dandy, J. Appl. Phys. **74**, 5803 (1993).

[26] S.J. Harris and L.R. Martin, J. Mater. Res. **5**, 2313 (1990).

[27] L.R. Martin and M.W. Hill, Appl. Phys. Lett. **55**, 2248 (1989).

[28] L.R. Martin and M.W. Hill, J. Mater Sci. Lett. **9**, 621 (1990).

[29] S.P. Chauhan, J.C. Angus, and N.C. Gardner, J. Appl. Phys. **47**, 4746 (1976); S.P. Chauhan, Thesis, Case Institute of Technology, 1972.

[30] S.J. Harris, J. Appl. Phys. **65**, 3044 (1989).

[31] D.W. Brenner, D.H. Robinson, R.J. Carty, D. Srivastava, and B.J. Garrision, in *Computational Methods in Materials Science*, edited by J.E. Mark, M.E. Glickman, and S.P. Marsh (Materials Research Society, Pittsburgh, PA 1992), pp. 255-260.

[32] D.W. Brenner, Phys. Rev. B **42**, 9458 (1990).

[33] L. Kostadinov and D. Dobrev, Surf. Coat. Technol. **47**, 623 (1991).

[34] M. Mulbrandon, private communication, 1995.
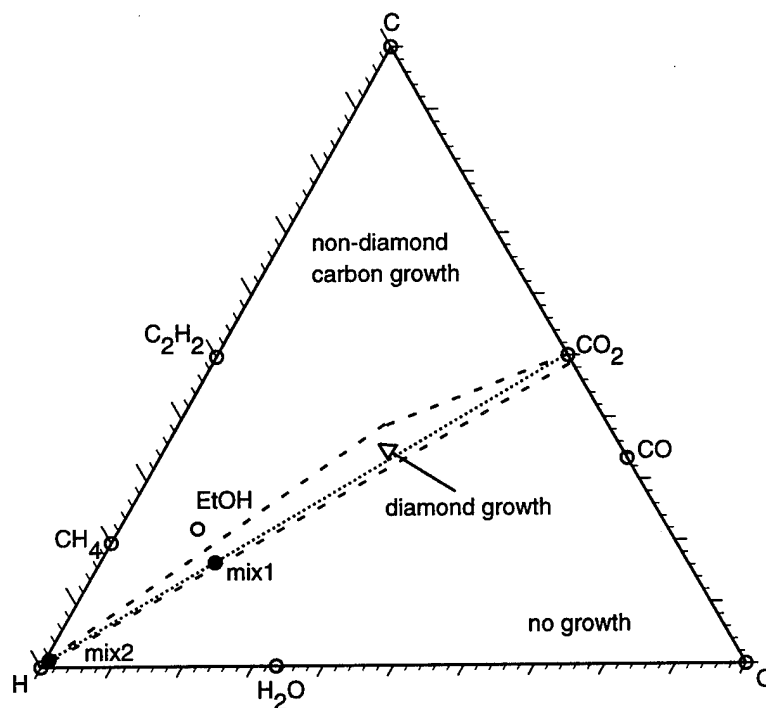
Fig. 1. C-H-O Ternary diagram. Dashed lines, adapted from ref. [1], indicate approximate locations of boundaries separating "diamond growth" domain from "no growth" and "non-diamond growth" domains. Dotted line is the CO-line and represents stoichiometries with equal mole fractions of carbon and oxygen. Open circles represent locations of pure compounds and filled circles indicate CO-rich (mix1) and CO-lean (mix2) stoichiometries investigated in this work.
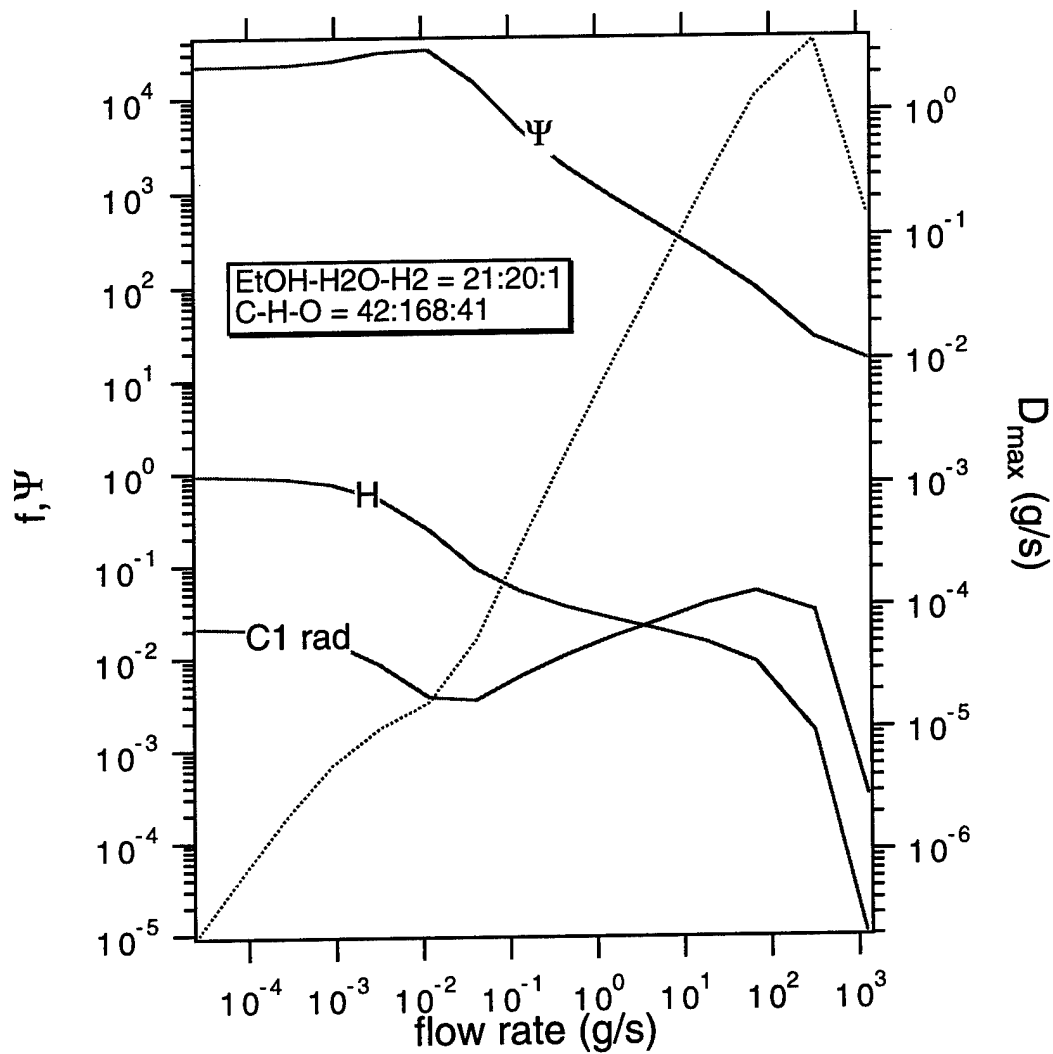
Fig. 2. Results of PSR calculations for ethanol-water-hydrogen 21:20:1. (a) Quality factor, f (C_1rad), f (H), and maximum growth rate (dotted line, plotted against right axis) versus flow rate, (b) carbon and hydrogen distributions versus flow rate.
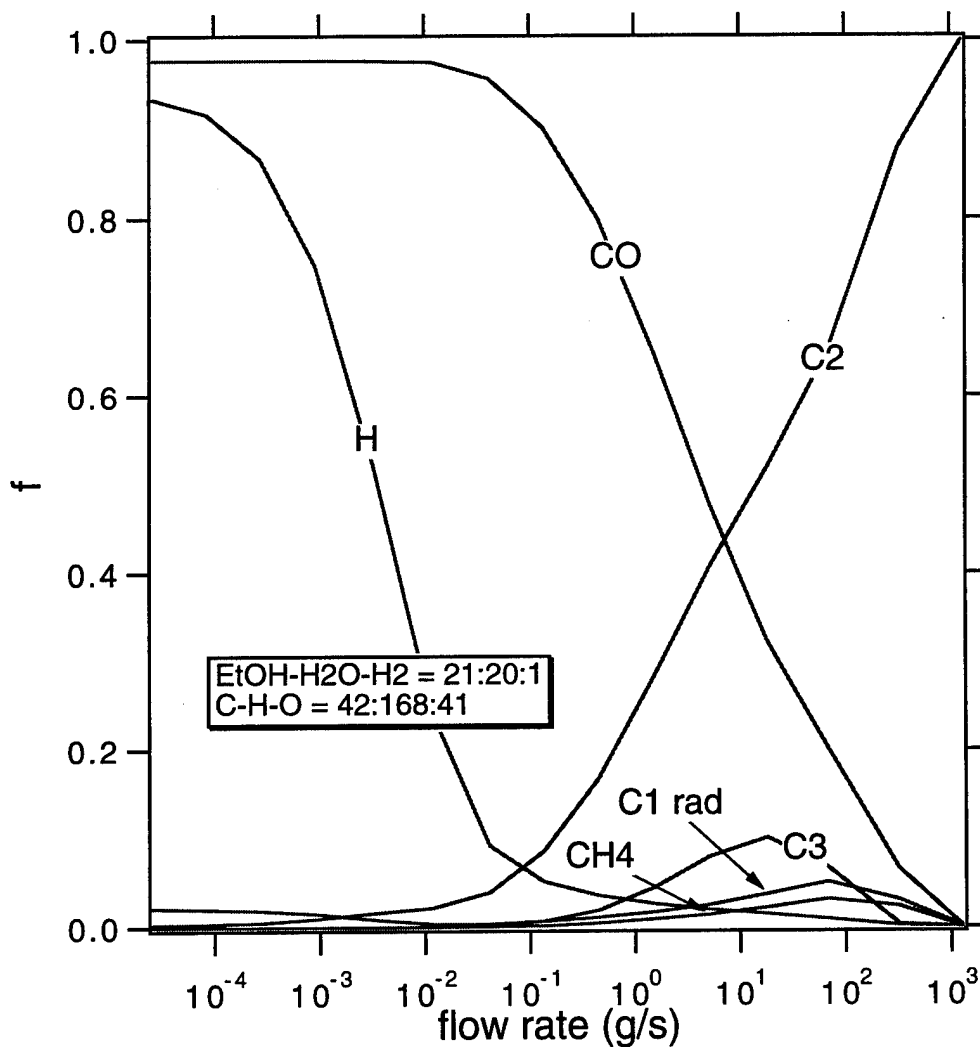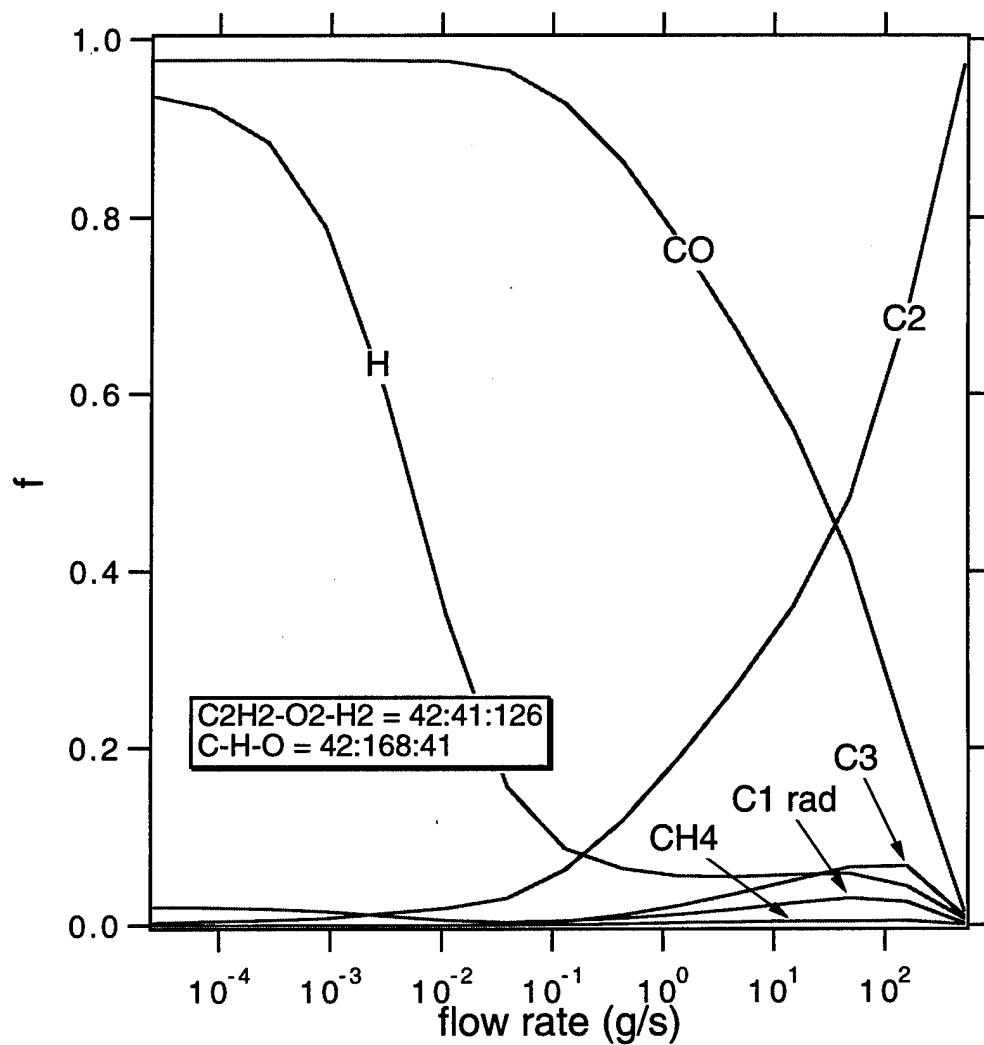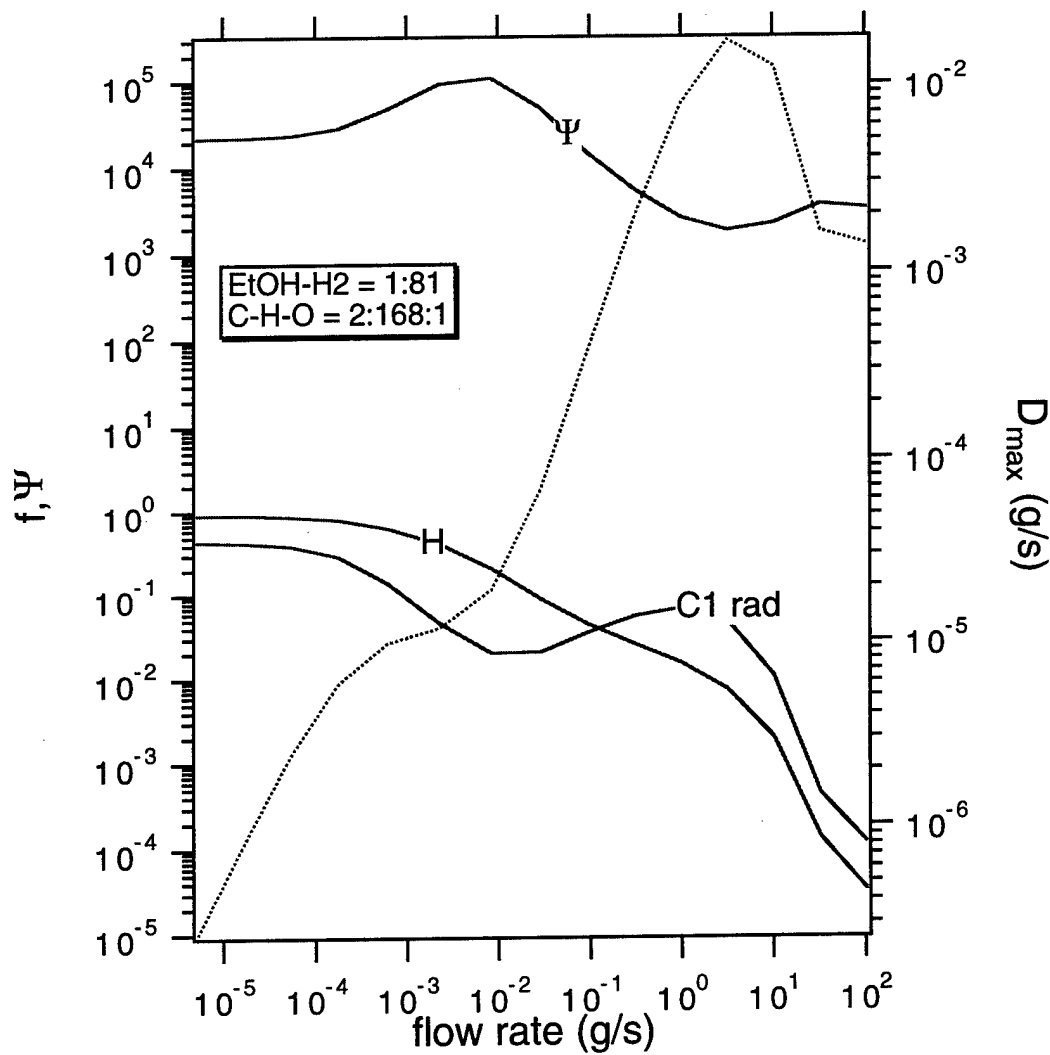
Fig. 2. (continues) Results of PSR calculations for ethanol-water-hydrogen 21:20:1. (a) Quality factor, $f(C_1rad)$, $f(H)$, and maximum growth rate (dotted line, plotted against right axis) versus flow rate, (b) carbon and hydrogen distributions versus flow rate.
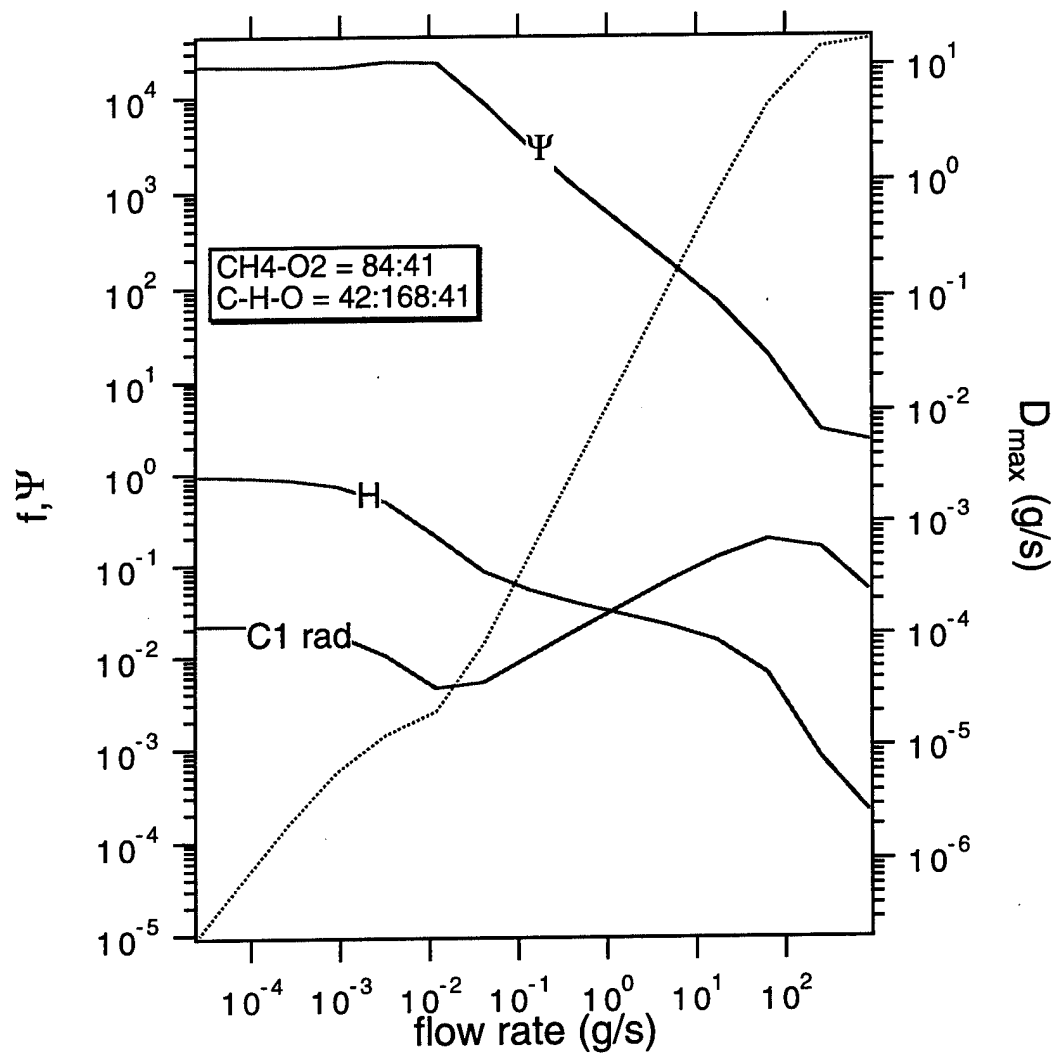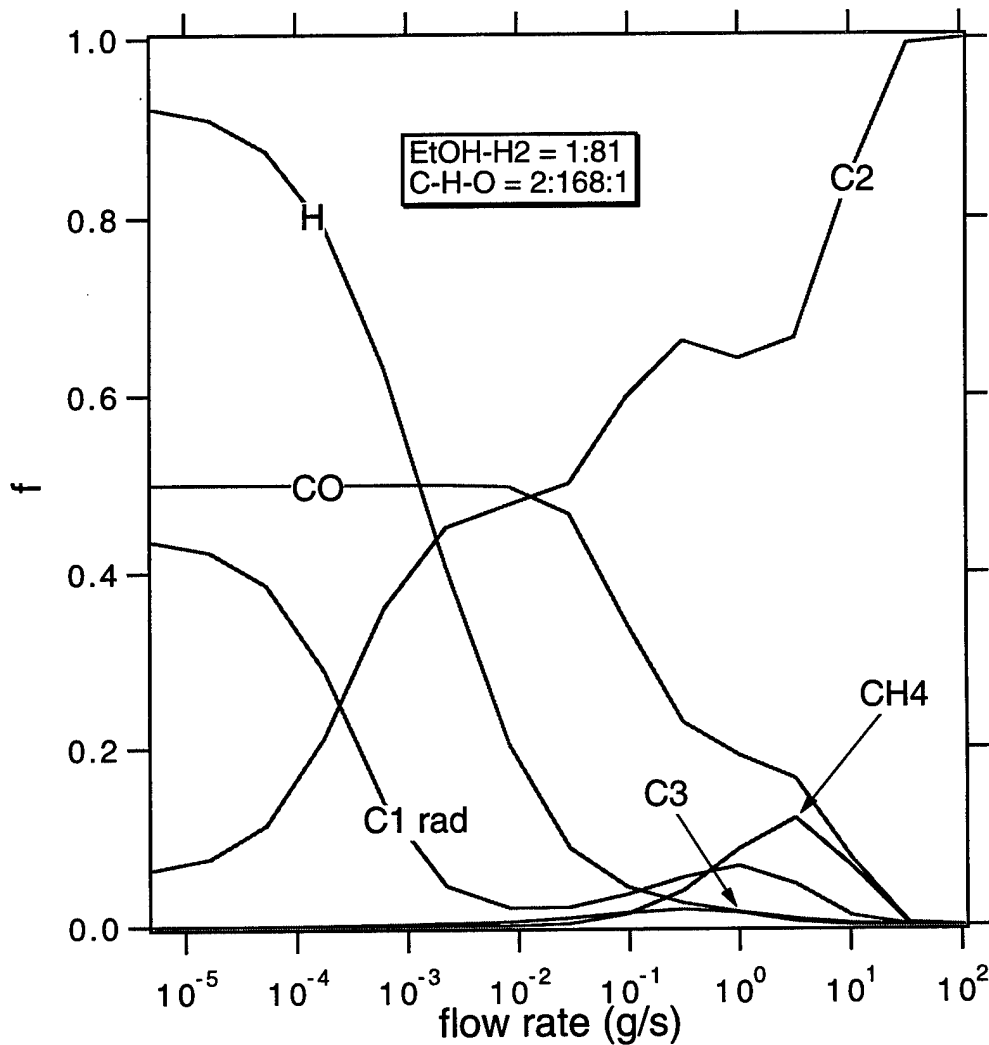
Fig. 3. Results of PSR calculations for methane-oxygen 84:41. (a) Quality factor, f (C_1rad), f (H), and maximum growth rate (dotted line, plotted against right axis) versus flow rate, (b) carbon and hydrogen distributions versus flow rate.
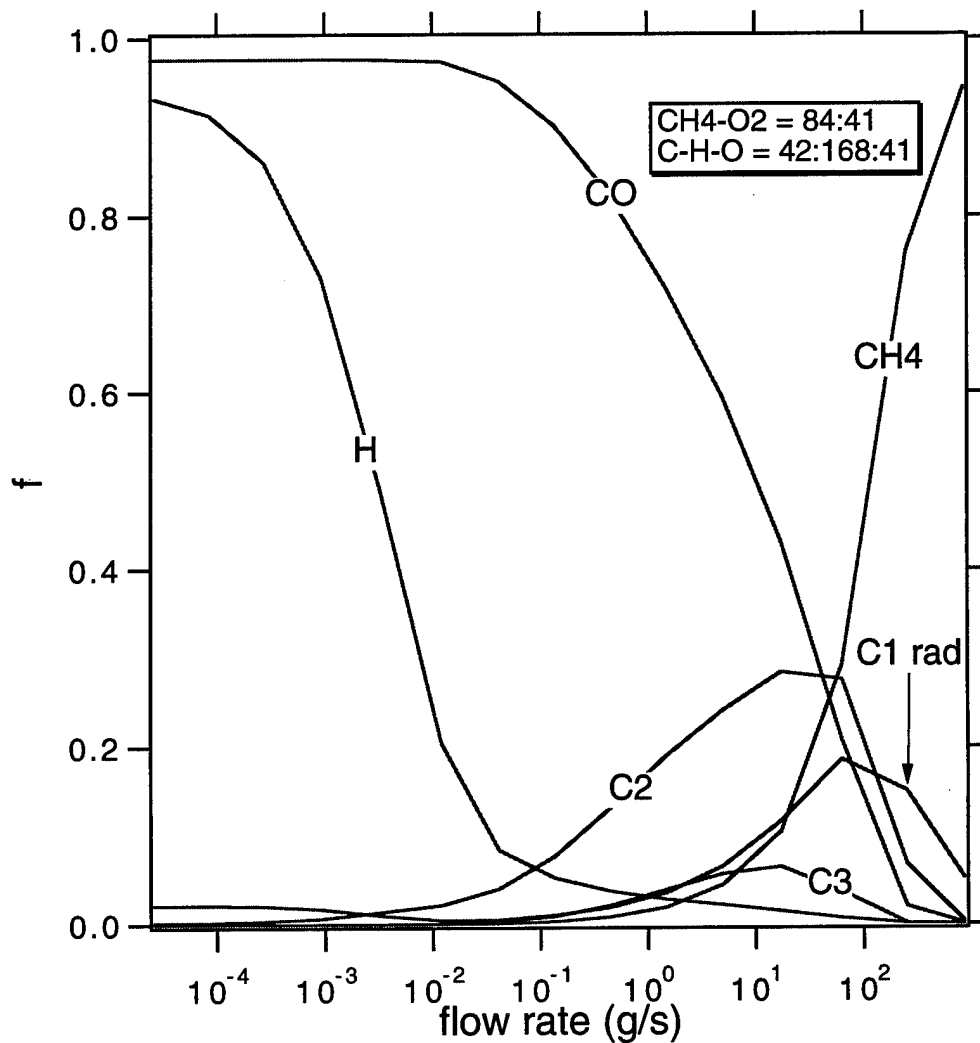
Fig. 3. (continues) Results of PSR calculations for methane-oxygen 84:41. (a) Quality factor, $f(C_1\text{rad})$, $f(H)$, and maximum growth rate (dotted line, plotted against right axis) versus flow rate, (b) carbon and hydrogen distributions versus flow rate.
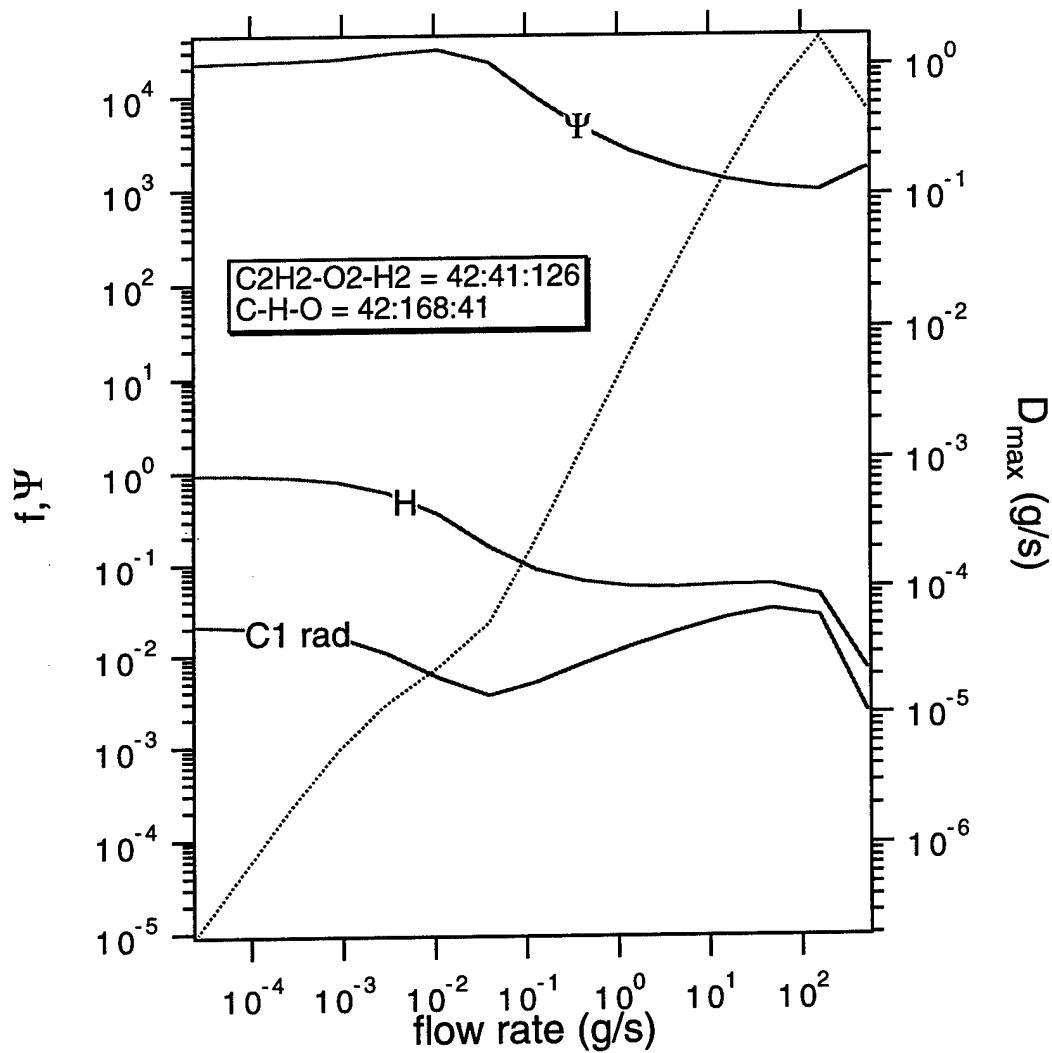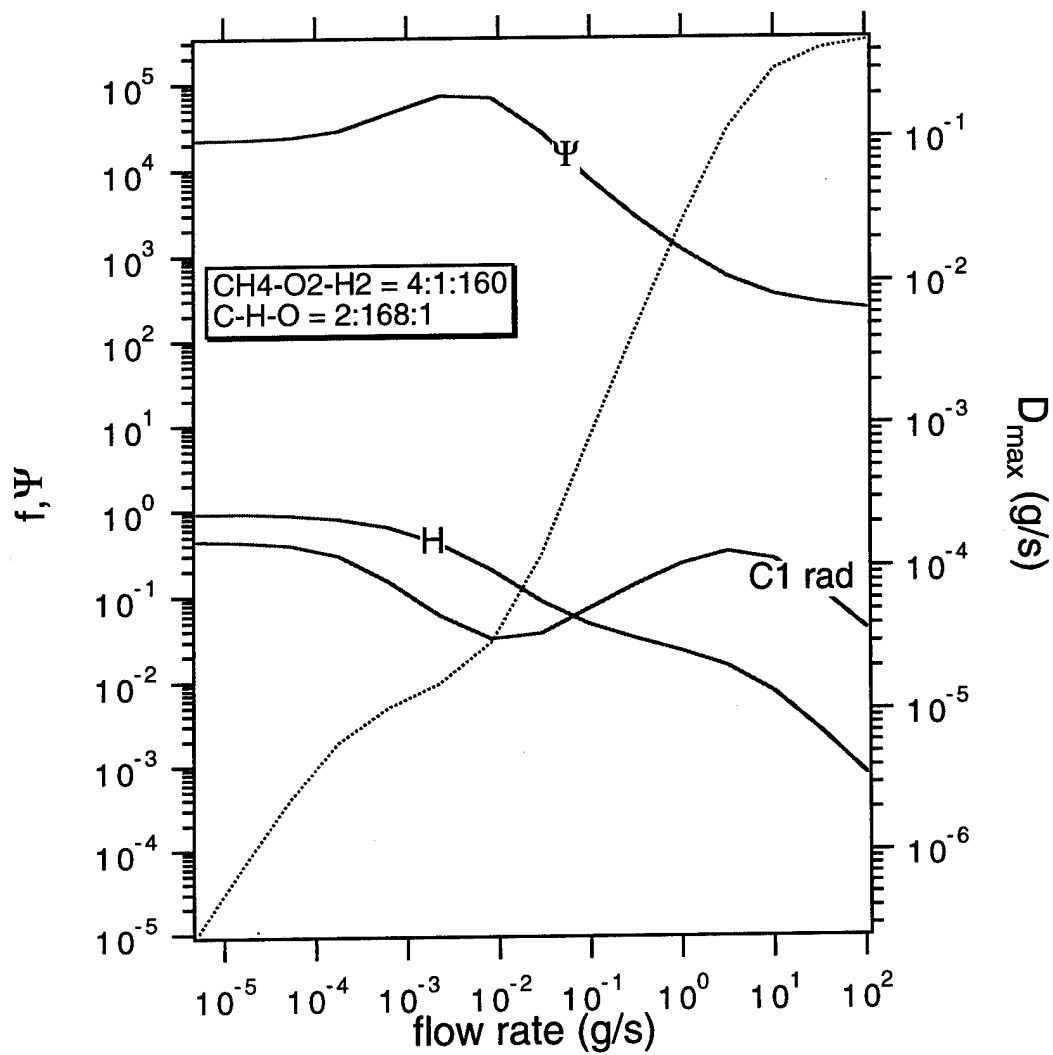
Fig. 4. Results of PSR calculations for acetylene-oxygen-hydrogen 42:41:126. (a) Quality factor, $f(C_1rad)$, $f(H)$, and maximum growth rate (dotted line, plotted against right axis) versus flow rate, (b) carbon and hydrogen distributions versus flow rate.
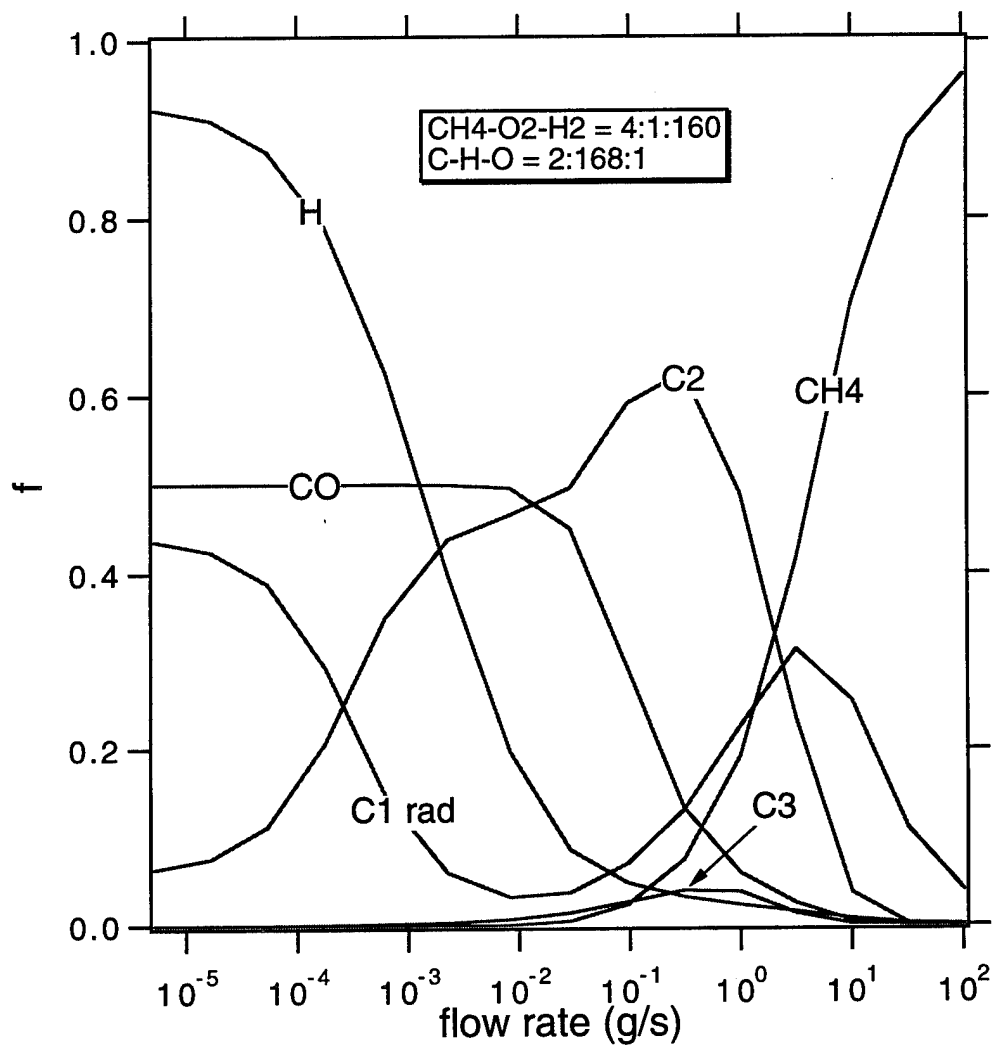
Fig. 4. (continues) Results of PSR calculations for acetylene-oxygen-hydrogen 42:41:126. (a) Quality factor, $f(C_1 rad)$, $f(H)$, and maximum growth rate (dotted line, plotted against right axis) versus flow rate, (b) carbon and hydrogen distributions versus flow rate.

Fig. 5. Results of PSR calculations for ethanol-hydrogen 1:81. (a) Quality factor, f (C_1rad), f (H), and maximum growth rate (dotted line, plotted against right axis) versus flow rate, (b) carbon and hydrogen distributions versus flow rate.
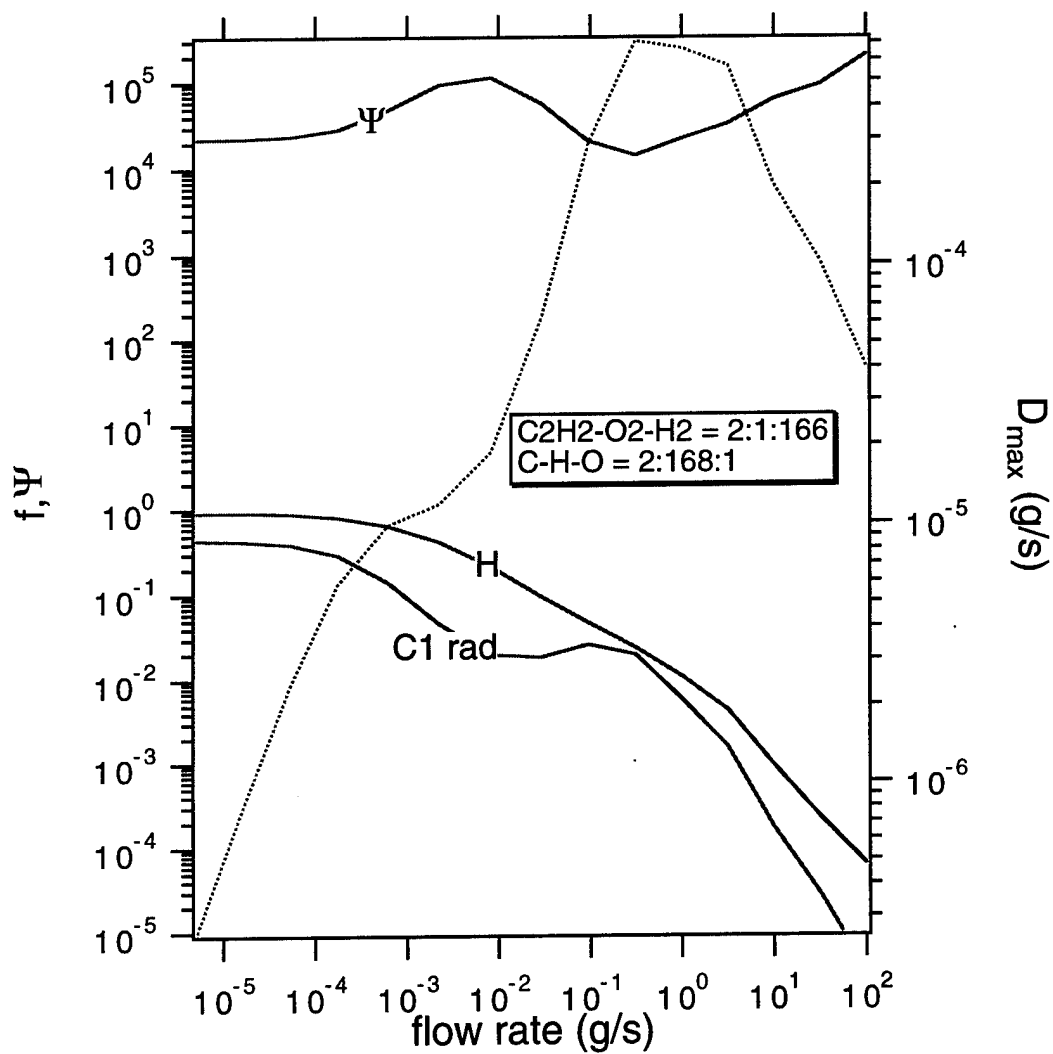
Fig. 5. (continues) Results of PSR calculations for ethanol-hydrogen 1:81. (a) Quality factor, f (C_1rad), f (H), and maximum growth rate (dotted line, plotted against right axis) versus flow rate, (b) carbon and hydrogen distributions versus flow rate.
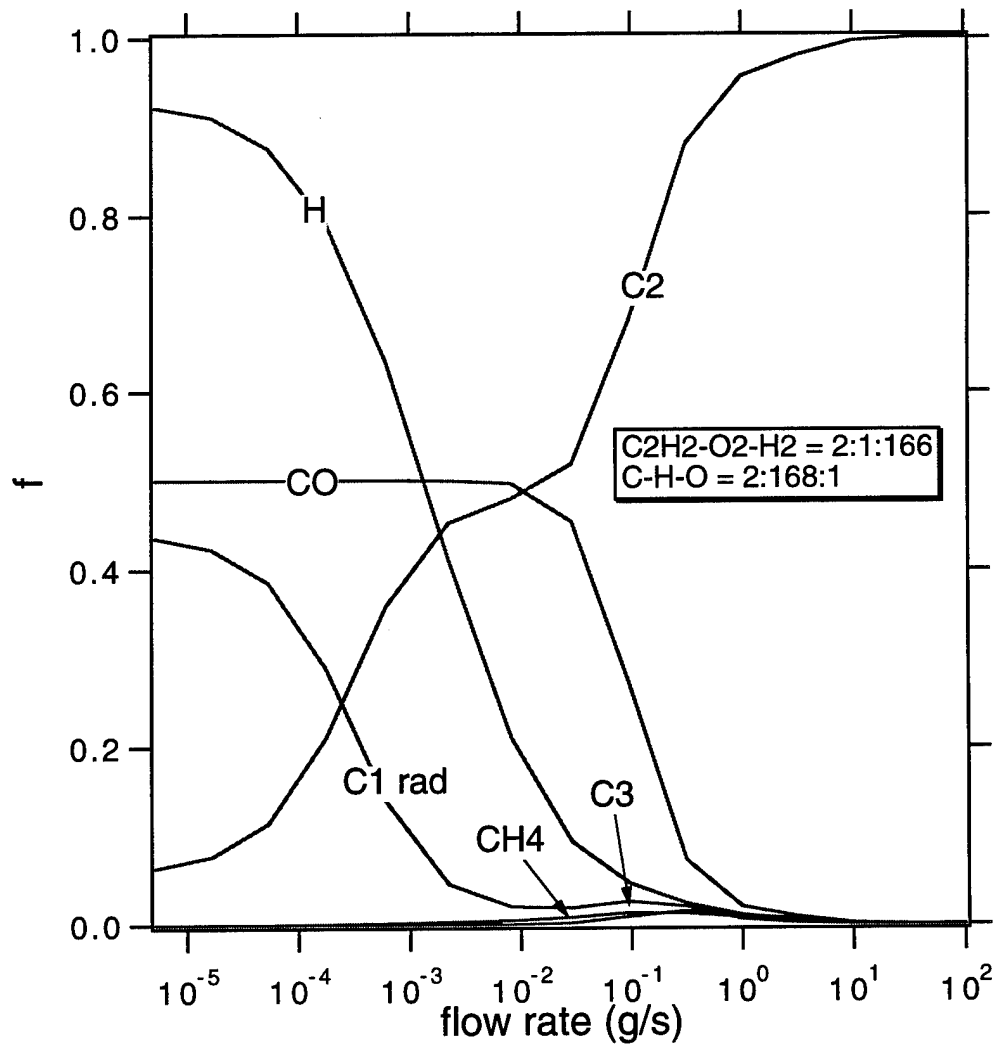
Fig. 6. Results of PSR calculations for methane-oxygen-hydrogen 4:1:160. (a) Quality factor, $f(C_1 \text{rad})$, $f(H)$, and maximum growth rate (dotted line, plotted against right axis) versus flow rate, (b) carbon and hydrogen distributions versus flow rate.

Fig. 6. (continues) Results of PSR calculations for methane-oxygen-hydrogen 4:1:160. (a) Quality factor, $f(C_1rad)$, $f(H)$, and maximum growth rate (dotted line, plotted against right axis) versus flow rate, (b) carbon and hydrogen distributions versus flow rate.

Fig. 7. Results of PSR calculations for acetylene-oxygen-hydrogen 2:1:166. (a) Quality factor, $f\,(C_1\text{rad}), f\,(H)$, and maximum growth rate (dotted line, plotted against right axis) versus flow rate, (b) carbon and hydrogen distributions versus flow rate.

Fig. 7. (continues) Results of PSR calculations for acetylene-oxygen-hydrogen 2:1:166. (a) Quality factor, $f(C_1rad)$, $f(H)$, and maximum growth rate (dotted line, plotted against right axis) versus flow rate, (b) carbon and hydrogen distributions versus flow rate.
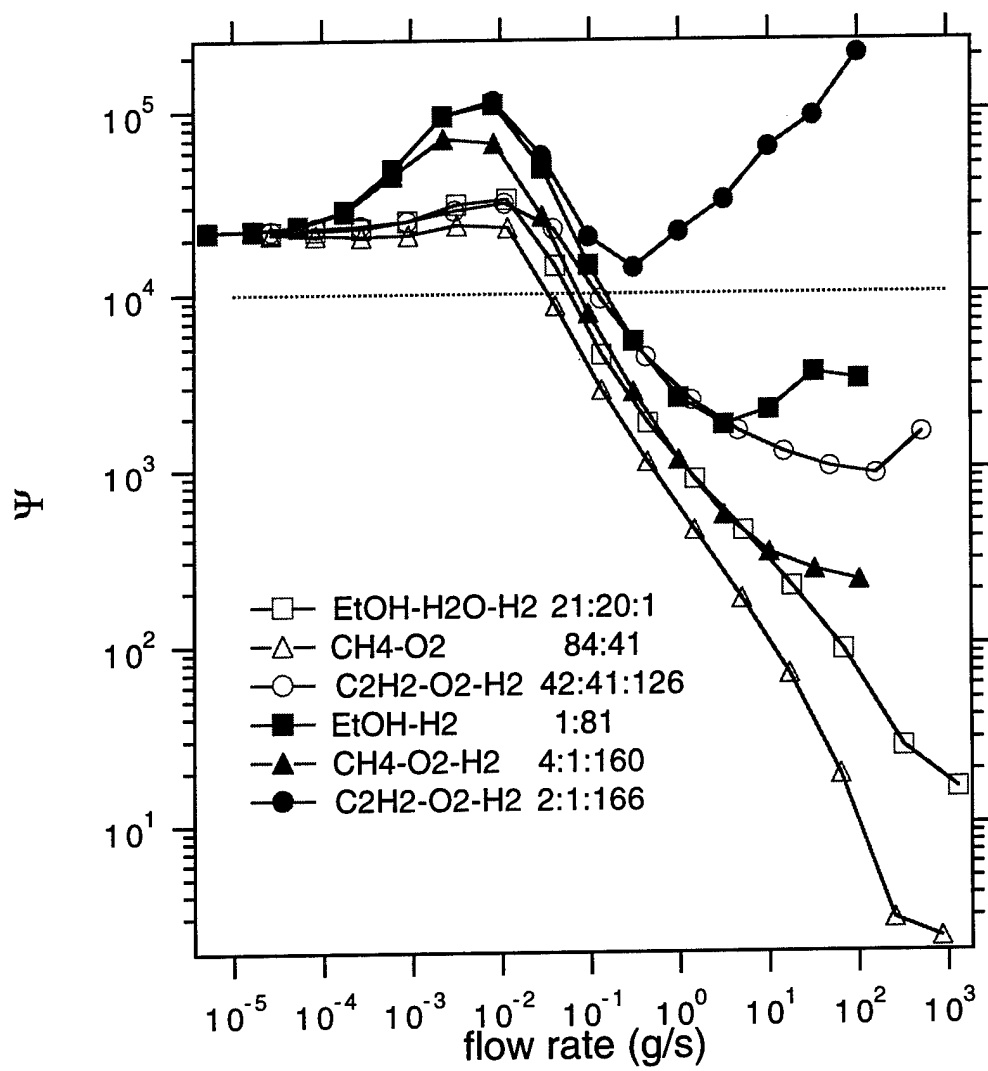
Fig. 8. Quality factors for the six different source-gas mixtures versus flow rate.
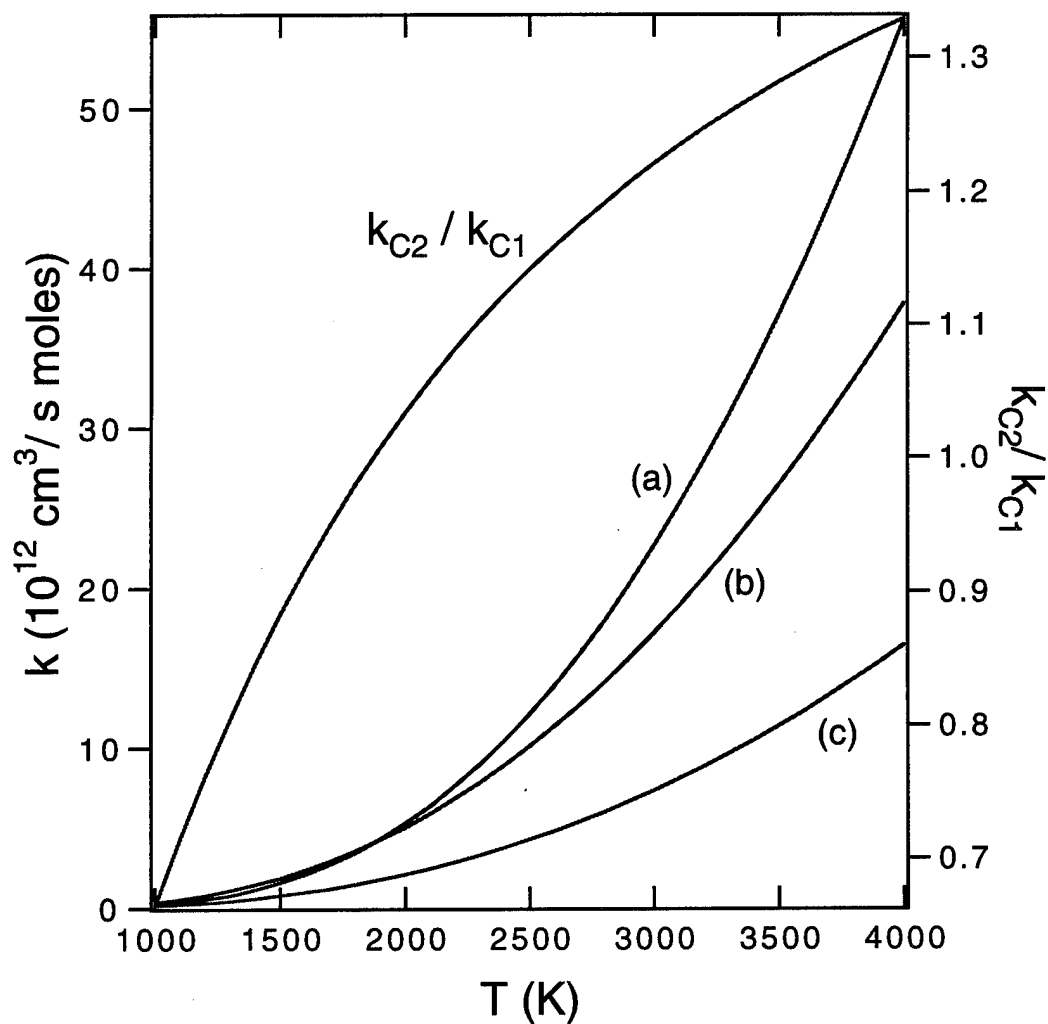
Fig. 9. Arrhenius rates for hydrogen atom-ethanol reactions yielding products (a) pC_2H_4OH, (b) sC_2H_4OH, (c) C_2H_5O or C_2H_5, and branching ratio (plotted against right axis) between reactions leading to C_1 and C_2 hydrocarbon formation versus temperature.
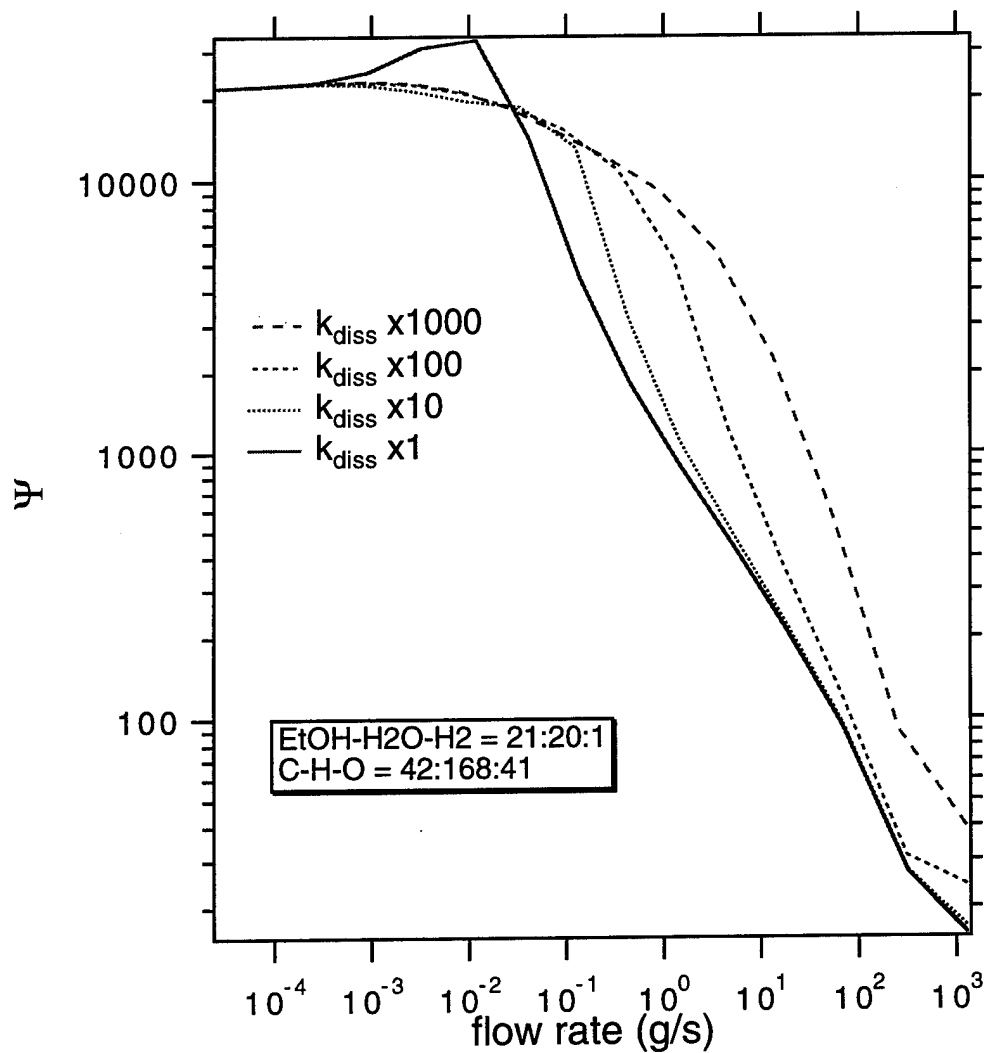
37

Fig. 10. Results of PSR calculations for ethanol-water-hydrogen 21:20:1 at various H_2 dissociation rates. (a) Quality factors and (b) maximum growth rates.
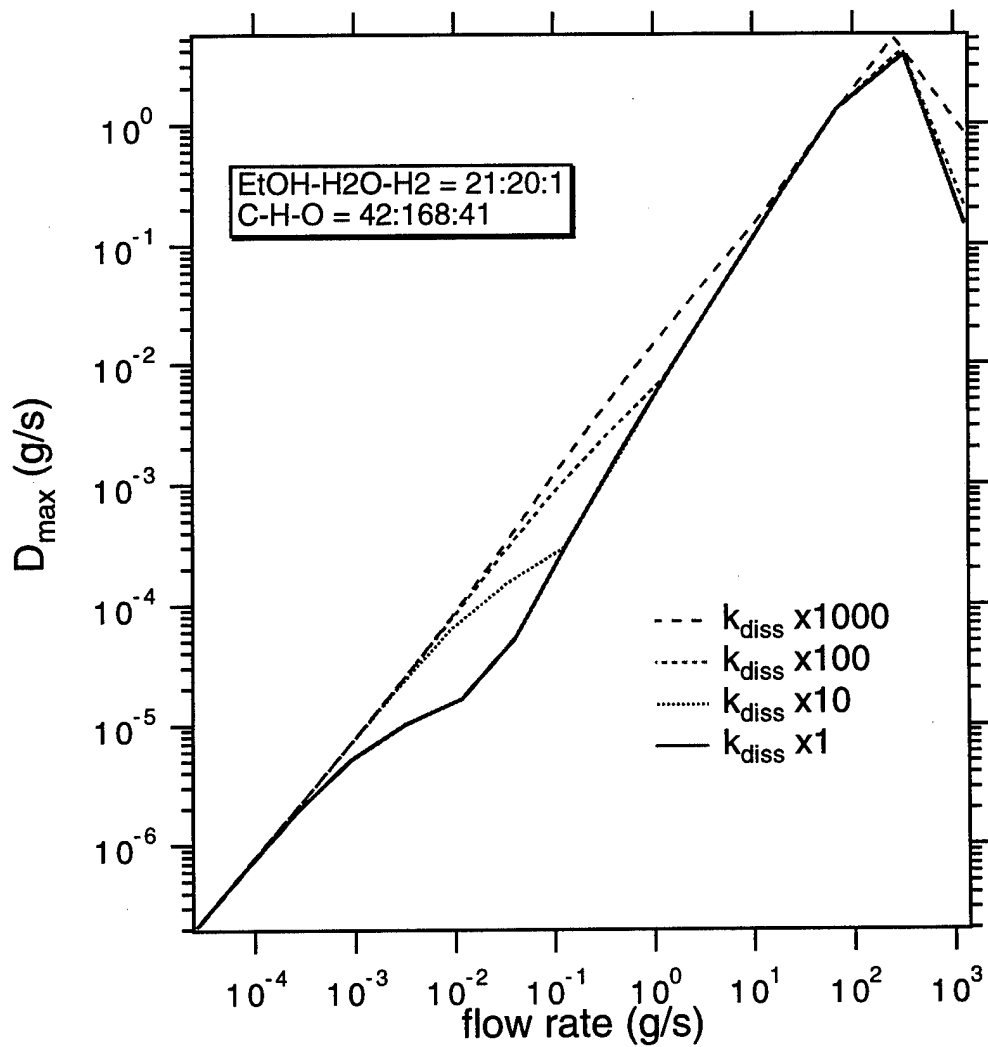
Fig. 10. (continues) Results of PSR calculations for ethanol-water-hydrogen 21:20:1 at various H_2 dissociation rates. (a) Quality factors and (b) maximum growth rates.
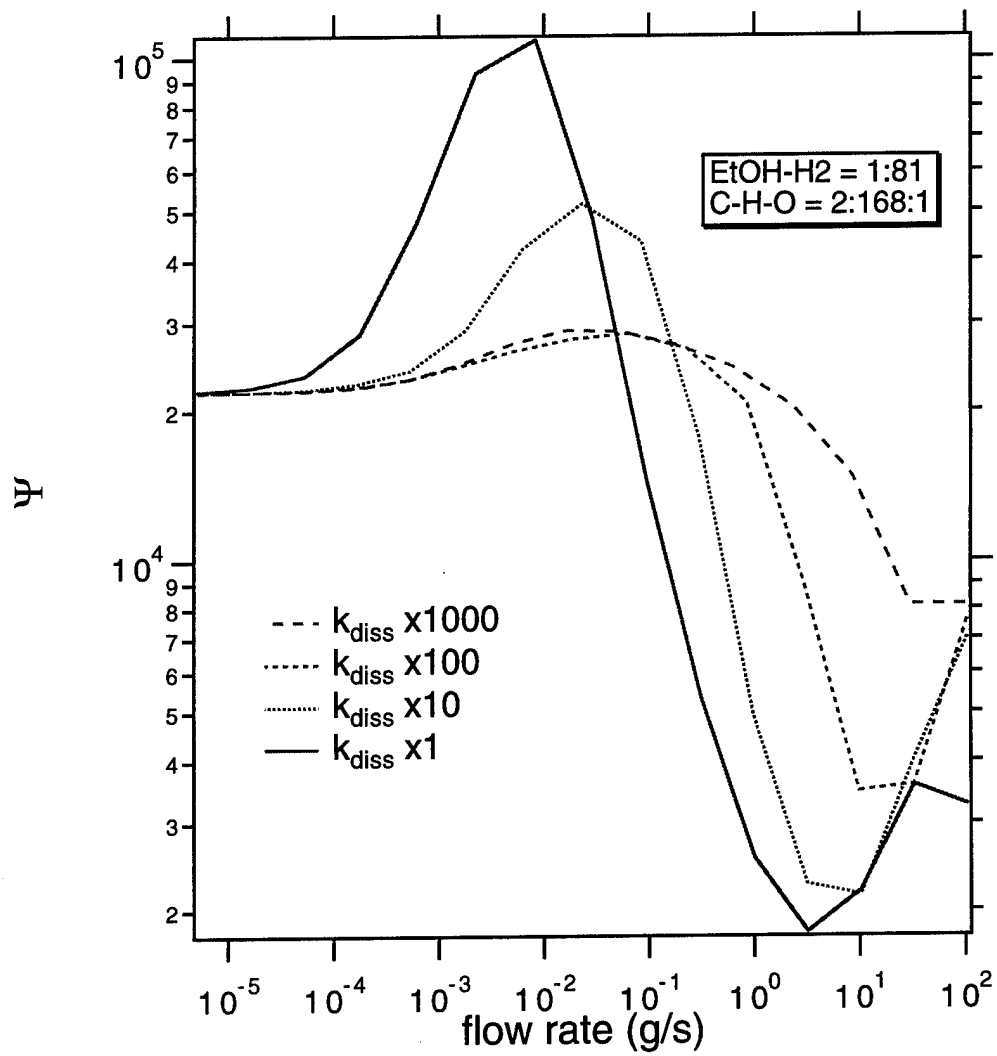
Fig. 11. Results of PSR calculations for ethanol-hydrogen 1:81 at various H_2 dissociation rates. (a) Quality factors and (b) maximum growth rates.
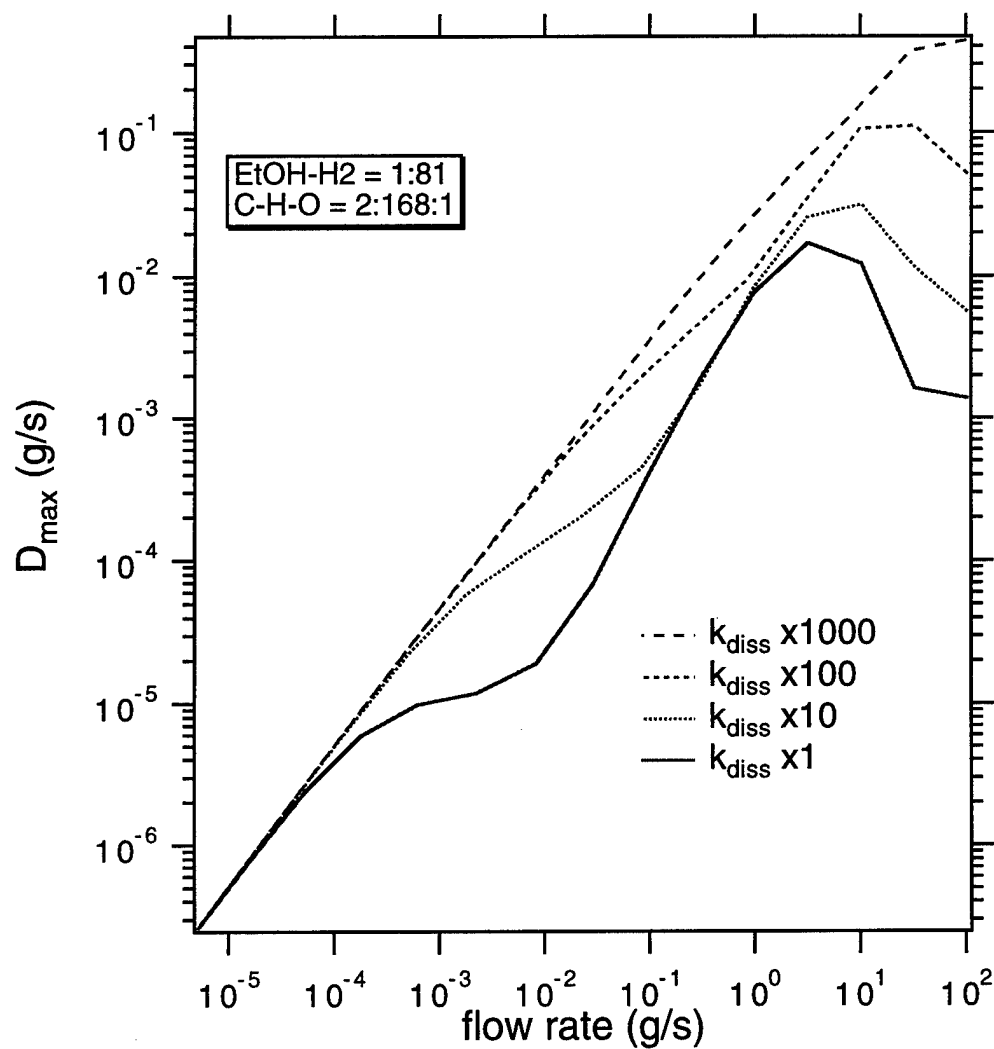
Fig. 11. (continues) Results of PSR calculations for ethanol-hydrogen 1:81 at various H_2 dissociation rates. (a) Quality factors and (b) maximum growth rates.